Design, fabrication and characterization of composite piezoelectric ultrafine fibers for cochlear stimulation

Carlos Mota [a,b], Massimiliano Labardi [c], Luisa Trombi [a], Laura Astolfi [d], Mario D'Acunto [e], Dario Puppi [b], Giuseppe Gallone [f], Federica Chiellini [b], Stefano Berrettini [a,g], Luca Bruschini [a,g], Serena Danti [a,f,*]

[a] OtoLab, Otorhinolaryngology, Audiology & Phoniatrics Unit, Azienda Ospedaliero-Universitaria Pisana (AOUP), Pisa, Italy

[b] BIOLab, Dept. of Chemistry and Industrial Chemistry, UdR INSTM Pisa, University of Pisa, Pisa, Italy

[c] Institute for Chemical-Physical Processes, National Research Council (CNR-IPCF), Pisa, Italy

[d] Bioacoustics Research Laboratory, Dept. of Neurosciences, University of Padua, Padua, Italy

[e] Institute of Science of Matter, National Research Council (CNR-ISM), Rome, Italy

[f] Dept. of Civil and Industrial Engineering, University of Pisa, Pisa, Italy

[g] Dept. of Surgical, Medical, Molecular Pathology and Emergency Medicine, University of Pisa, Pisa, Italy

* Correspondence to:
Serena Danti, Dept. of Civil and Industrial Engineering, Largo L. Lazzarino 2, 56122 Pisa, Italy. E-mail: serena.danti@unipi.it

Keywords: electrospinning; barium titanate; polyvinylidene fluoride; aligned fibers; neural cells; transducer.

Conflict of interest: All the authors declare to have no conflicts of interest related to this study.

Contributions: CM, ML, MD, LT, AL, DP, SD performed experiments; CM, ML, MD, GG, FC, SD analyzed data; FC, SB provided materials and equipment; CM, LB, SD designed the study; CM and SD wrote the manuscript. All the authors read and approved the final version of article.

Abstract

Sensorineural hearing loss, primed by dysfunction or death of hair cells in the cochlea, is the main cause of severe or profound deafness. Piezoelectric materials work similarly to hair cells, namely, as mechano-electrical transducers. Polyvinylidene fluoride (PVDF) films have demonstrated potential to replace the hair cell function, but the obtained piezoresponse was insufficient to effectively stimulate the auditory neurons. In this study, we reported on piezoelectric nanocomposites based on ultrafine PVDF fibers and barium titanate nanoparticles (BTNPs), as a strategy to improve the PVDF performance for this application. BTNP/PVDF fiber meshes were produced via rotating-disk electrospinning, up to 20/80 weight composition. The BTNP/PVDF fibers showed diameters ranging in 0.160-1.325 μm. Increasing collector velocity to 3000 rpm improved fiber alignment. The piezoelectric β phase of PVDF was well expressed following fabrication and the piezoelectric coefficients increased according to the BTNP weight ratio. The BTNP/PVDF fibers were not cytotoxic towards cochlear epithelial cells. Neural-like cells adhered to the composite fibers and, upon mechanical stimulation, showed enhanced viability. Using BTNP filler for PVDF matrices, in the form of aligned ultrafine fibers, increased the piezoresponse of PVDF transducers and favored neural cell contact. Piezoelectric nanostructured composites might find application in next generation cochlear implants.

1 Introduction

Sensorineural hearing loss (SNHL) is a major impairment of the inner ear as a consequence of damaged sensory epithelium. These cells, known as hair cells, are present in the organ of Corti to convert mechanical vibration of the basilar membrane into electric stimulation of the underlying neurons. Dysfunction of the mechano-electrical transduction capability of hair cells leads to deafness. Although ageing or external factors, such as exposure to noise and ototoxic effects of certain drugs, can affect the viability and function of the hair cells, in most cases (> 60%) SNHL is associated to inherited genetic conditions [1-3]. To treat SNHL, several approaches, such as gene therapies, stem cell-based treatments, neuroprotective and chemical drugs, are being investigated aimed at the regeneration of the delicate inner ear microenvironment [3, 4]. Despite of these new biological and pharmaceutical strategies, nowadays, the only successful treatment for SNHL still relies on the use of cochlear implants (CIs), which involve an invasive and complex surgery of the temporal bone [2]. The CI is a multi-component electronic device that completely replaces the ear function. It includes an external receiver powered by a battery in which the sound is captured and processed and finally transmitted to a subcutaneous receiver that is connected to the electrode array implanted inside the cochlea [5]. The electrode array directly stimulates the auditory nerves, bypassing the need for hair cells as transducers. Since the fifties, different electrode arrays have been developed, composed with a variable number of electrodes and configurations; however, so far, tone recognition of speech or music remains the pinnacle of CI-implanted patients [6, 7].

Piezoelectric materials have recently been explored in diverse fields, including biomedicine and energy harvesting [8, 9]. The development of novel CIs evolving towards the utilization of piezoelectric materials was firstly suggested by Mukherjee *et al.* at the beginning of this century [10-12]. Unlike conventional CIs, piezoelectric CIs are not ferromagnetic and exploit the cochlear constitutive mechanical tonotopy (i.e. frequency selectivity along the main axis of the basilar membrane), enabling a fine tuning process of the sound vibrations [13]. Frequency selectivity, travelling waves and tonotopic organization in an artificial membrane have been demonstrated [14]. Indeed, according to the travelling wave theory, tuning for sound frequency is largely determined by position. A piezoelectric polymeric film made of polyvinylidene fluoride (PVDF) was able to work as a stand-alone device, namely, without the necessity of an external power supply, thus resulting extremely appealing to reproduce an artificial cochlea [14]. For the fabrication of cochlear microdevices that must be flexible to accommodate the curvy inner ear anatomy, PVDF is indeed an interesting material, as it owns good piezoelectric properties together with the excellent processability proper of polymers [15, 16]. The development of PVDF-based film membranes for

cochlear stimulation has become a subject of few recent studies, showing the potential of changing the future way of treating SNHL, even though an insufficient sensitivity has been reached so far using plain PVDF [11, 14, 17].

On the other hand, ceramic materials with a perovskite-like structure, possess higher piezoelectric properties than those of polymers, but are very rigid and difficult to process. Among them, barium titanate ($BaTiO_3$) is a ceramic with excellent piezoelectric properties routinely applied in devices such as piezoelectric actuators and capacitors [18]. In recent years, barium titanate has also become a subject of biological and biomedical studies [19]. First evidences have shown that $BaTiO_3$ nanoparticles (BTNPs) were biocompatible and could be uptaken by cells with neither inducing apoptosis nor affecting cell metabolism and viability. BTNPs were also used as a filler for polymeric-matrix biomedical composite and as a carrier for an anticancer drug, thus appearing a versatile tool in biomedical applications [20]. It has also been demonstrated that BTNPs increased the piezoelectric properties of films made of a PVDF family copolymer [21].

To maximize the efficiency of a piezoelectric substrate toward the resident neural cells, an effective nanoscale contact between the neurites and the material must occur, which sometimes is difficult to achieve by using non-porous flat substrates, like films. Uniaxially aligned fibrous materials have shown topographic features providing favorable interactions with neurons and showing the ability to direct neurites [22]. Electrospinning is a widely used technique to manufacture fibrous materials for variety of applications, such as nanofiber-reinforced composites, membranes, smart cloths, electrode materials, sensors, as well as electronic and optical devices [23-25]. In the biomedical field, this techniques has gained a large popularity for its simplicity, cost-effectiveness and ability to produce nano-sized fibers resembling those of the native extracellular matrix, thus showing architectural cues suitable for cell interaction [26, 27]. Electrospun fibers can be produced with diameters ranging from a few micrometers down to tens of nanometers, leading to meshes that present superior surface area-to-volume ratios. Specifically, electrospinning offers several theoretical advantages for producing piezoelectric substrates for cochlear stimulation: *(i)* it allows the fabrication of ceramic/polymer nanocomposites by incorporating nanoparticles in the polymeric solution, *(ii)* it inherently induces a poling effect on the piezoelectric fibers during the spinning process by means of the high electric field necessary for manufacturing, and finally *(iii)* it permits fiber deposition geometry to be tuned, which can be of outmost importance to induce specific cellular signals.

The aim of this study was the production of aligned ultrafine PVDF/BTNP piezoelectric fiber meshes via electrospinning with increased piezoelectric properties with respect to the plain PVDF and with morphological nano/micro features attractive for neural cells, as a step forward towards

the accomplishment of piezoelectric substrates for CIs. Fiber morphology and alignment were evaluated via scanning electron microscopy (SEM) and two-dimensional Fast Fourier Transform (FFT), whereas single fiber topography was investigated via atomic force microscopy (AFM) and scanning near optical microscopy (SNOM). The dispersion of BTNPs inside the composite fibers was investigated using scanning transmission electron microscopy (STEM). The crystallographic and compositional characterization of the composite was performed via X-ray diffraction (XRD) and attenuated total reflectance Fourier transform infrared spectroscopy (ATR-FTIR). The mechanical behavior of the composite was tested under *in situ* environmental SEM (ESEM) tensile deformation and dynamic-mechanic thermal analysis (DMTA). Piezoelectric coefficients were evaluated as a function of BTNP concentration in the polymer using a custom-made bench apparatus. Finally, the composite material was cultured *in vitro* with inner ear epithelial cells to assess its cytocompatibility, and with neural-like cells using a bioreactor capable of imparting cyclic bending solicitation during cell culture, as a preliminary test to support its possible application in CI.

Advancements in the development of high performance piezoelectric biomaterials to be used as cochlear transducers would allow SNHL treatment to move forward the next generation CIs. Changing from electronics-based to biomaterials-based CIs, the latter being cost-effective, simple, biomimetic, water and magneto-compatible, would drastically improve the quality of life of deaf people.

2 Materials and methods

2.1 Materials

PVDF (Solef 11008) was kindly provided by Solvay Specialty Polymers S.p.A (Rosignano Solvay, LI, Italy) and barium titanate ($BaTiO_3$) nanoparticles with an average particle size of 100 nm were acquired from Nanostructured & Amorphous Materials, Inc. (Houston, TX, USA) [28]. Dimethylformamide (DMF) and acetone were supplied by Sigma Aldrich (Milan, Italy).

2.2 Preparation of polymeric solutions

PVDF powder at a concentration of 20% w/v was dissolved in a mixture of DMF and acetone (1:1 v/v) and stirred overnight [29]. For the preparation of composite electrospun fibers a selected amount of BTNPs ($BaTiO_3$/PVDF weight ratios of 0%, 10%, 15% and 20% w/w) was added to the polymer solution and vigorously stirred overnight. Moreover, before loading each composite

solution into the electrospinning syringe, these were further stirred by placement in an ultrasound bath (Bransonic 2510, Bransonic, Danbury, CT, USA), setting an output power of 20 W for 1 h to improve the dispersion of the nanoparticles.

2.3 Production of electrospun fiber meshes

Each polymeric solution was loaded into a 5 ml syringe, fitted with a blunt tip stainless steel needle (Gauge 21, inner diameter = 0.34 mm, length = 50 mm), and placed into the syringe pump (BSP-99 M, Braintree Scientific Inc., Braintree, MA, USA). A constant flow rate (F = 1 $ml \cdot h^{-1}$) was used for all the experiments. Two high voltage power supplies of opposite polarity (SL60PN300, Spellman High Voltage, UK) were applied. The needle was positively charged, whereas the counter electrode was negatively charged (**Figure 1**).

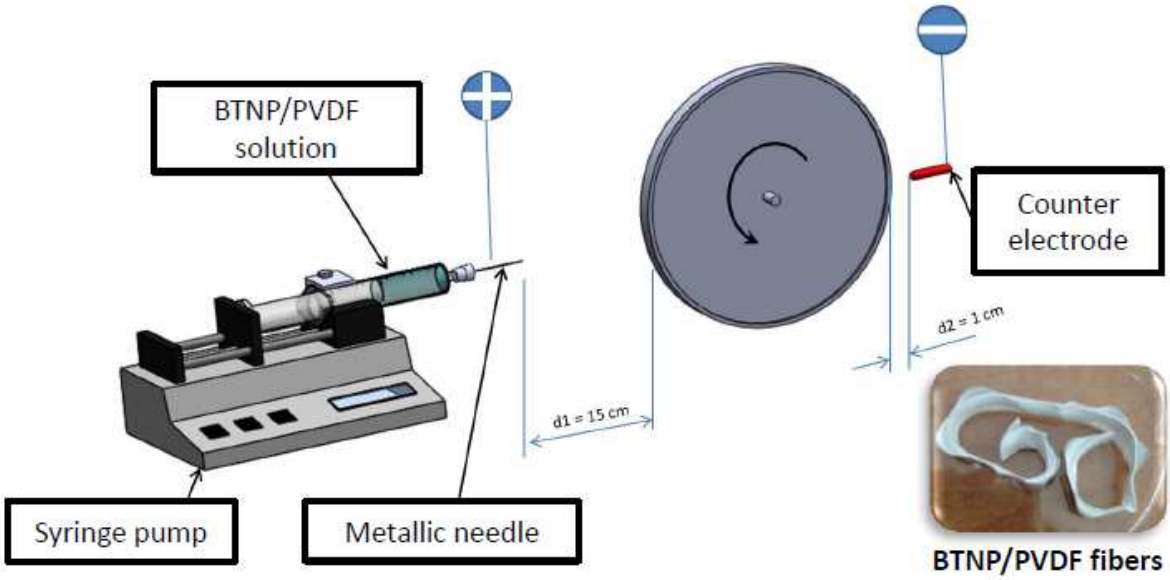

Figure 1. Scheme of the electrospinning apparatus used to produce the BTNP/PVDF fibers, with weight compositions 0/100, 10/90, 15/85 and 20/80.

A constant electrical potential difference (V) of 20 kV was generated by applying a positive voltage (10 kV) to the needle and a negative voltage (-10 kV) to the counter electrode. A rotating disk with a diameter of 14 cm was placed in between the needle and the counter electrode, respectively at 15 cm (d1) and 1 cm (d2) distances, and was used to collect the fibers. The distances d1 and d2 were kept constant for all the conducted experiments. The collection surface of the disk having 1 cm width was covered with an aluminum foil strip with the same dimension. The rotation velocity was changed from 500 to 3000 r.p.m, resulting in a variation of the tangential velocity (V_t) in the range of 3.7 to 22.0 $m \cdot s^{-1}$. The collection of the electrospun fibers was performed in 1 h. All the fabricated

meshes were dried under a fume hood and then kept in oven set at 60°C under vacuum for 72 h to fully remove the residual solvent. For each test performed, the number of samples tested for each composition (*n*) was reported.

2.4 Characterization of fiber morphology and topography

Electrospun fiber morphology was evaluated via SEM (EVO MA10, Carl Zeiss, Jena, Germany). The meshes (n = 3) were sputter-coated with gold (Emitech K550, Quorum Technologies Ltd., Laughton East Sussex, England) for 4 min prior to observation. SEM micrographs were acquired at different magnifications to visualize the details of interest. Fiber diameter was measured using ImageJ version 1.47h (http://rsbweb.nih.gov/ij/), and over 100 measurements were taken for each sample prepared. BTNP dispersion inside the fibers was evaluated via STEM. Composite BTNP/PVDF fibers were placed on a copper grid, mounted on the support and analyzed under STEM using a FEI Helios NanoLab™ 600 Dual Beam FIB/SEM (Hillsboro, Oregon, USA).

Topographic profiling of single fibers adhering onto the aluminum substrate was performed by tapping-mode AFM using a Veeco Instruments Multimode atomic force microscope equipped with Nanoscope IIIa controller. Non-contact mode silicon cantilevers were used (Veeco RTESP10, with 265-311 kHz nominal resonant frequency, and 20-80 N/m nominal spring constant).

In addition, fiber topography was imaged using a shear force system via SNOM (n = 4). Single electrospun fibers were tailored with a shear force apparatus based on a tuning fork feed-back as usually used in near-field optical microscopy. This technique operating in near contact allows single fiber topography to be measured with a probe by preventing a contact between microscopy tip and fiber that could generate artifacts and low quality imaging.

.

2.5 Evaluation of fiber alignment

Fiber alignment was evaluated using two-dimensional FFT method described by Ayres et al [25]. Briefly, .TIF image files (n = 3), as obtained via SEM, were edited with ImageJ software, converted into 8-bit and rotated in order to align with the collection direction. Images were cropped with 512×512 pixels and analyzed with FFT. The William O'Connell oval profile plug-in was used to measure pixel intensity performing the radial sum for each angle (0°-360°, 1° of increment). The results obtained were normalized to zero baseline and plotted with arbitrary units for each angle ranging from 0° to 180°.

2.6 Crystalline phase characterization of BTNP/PVDF fibers

XRD was used to investigate the presence of the piezoelectric crystalline phases β in BTNP/PVDF composites (n = 1). XRD patterns were recorded on BTNP/PVDF fibers using an X-ray powder diffractometer (Kristalloflex 810, Siemens, Munich, Germany) using Cu Kα radiation (λ = 1.5406 Å) at a scanning rate of 0.016° s^{-1} with 2θ ranging in 10°-80° and a temperature of 25°C.

ATR-FTIR was performed by using a Jasco FT-IR 410 (Jasco Europe, Italy) spectrophotometer to assess the influence played by the fabrication process on the PVDF crystalline phases α (non-piezoelectric) and β (piezoelectric) of the raw and processed polymer.

2.7 Mechanical characterization of BTNP/PVDF fibers

The mechanical behavior of BTNP/PVDF fiber meshes was qualitatively investigated via *in situ* ESEM (Zeiss, EVO MA15) tensile test, equipped with a single 2 kN lead screw calibrated at 200 N. Briefly, the sample (n = 1) was placed in the ESEM holders with a span of 10.0 mm preloaded at 0.052 N with motor speed set at 0.1 mm·min^{-1}. Subsequently, the motor speed was set at 0.05 mm·min^{-1}. At 2 min intervals during the tests, ESEM micrographs were taken under an electron beam set at 14.45 kV and of 501× magnification. Tensile tests were performed until the applied force (F) dropped down to zero (rupture). DMTA was carried out on a Gabo Eplexor® 100 N (Gabo Qualimeter® Testanlagen GmbH, Ahlden, Germany). The strips, about 3 cm long, were cut from the fiber ribbons. An approximate cross section area of each strip was measured using a thickness gauge and a caliper. A 1% pre-strain was applied and the dynamic strain was carried out at 0.1% in tensile mode. The tests were performed at 37°C and frequency range 0.1 - 100 Hz.

2.8 Piezoelectric characterization of BTNP/PVDF fibers

Piezoelectric transduction was measured on mesh strips of typical size 20 × 5 mm^2 (xy), obtained by overlaying of 4 to 5 mesh layers, in order to increase sample thickness and spring constant to allow proper handling and measurement stability. Samples were loaded in a home-made setup for piezoelectric strain measurement, briefly described in the following. One end of the sample was fixed to a holder, attached to a harmonic steel slab spring, referred to as the measurement spring, by means of Teflon clamps. The other end of the sample was attached to a small microtranslator, enabling pre-tension of the sample, by Teflon clamps. An electric potential could be applied in transverse direction (z) through a pair of metal slabs, positioned very close to the strip surface (xy). In this way, the transverse electric field produced a longitudinal deformation (along x) with magnitude proportional to the piezoelectric coefficient d_{31} of the material. Alternating electrical drive at the resonance frequency of the measurement spring produced an enhancement of its

vibration by a factor ranging from about 20 to 60, due to the harmonic oscillator quality factor *Q*. Bending of the steel slab was detected by the optical lever method, where a laser beam was reflected by a mirror attached on the spring and its deflection was detected by a four-quadrant split photodiode. The setup is schematically depicted in **Figure 2**.

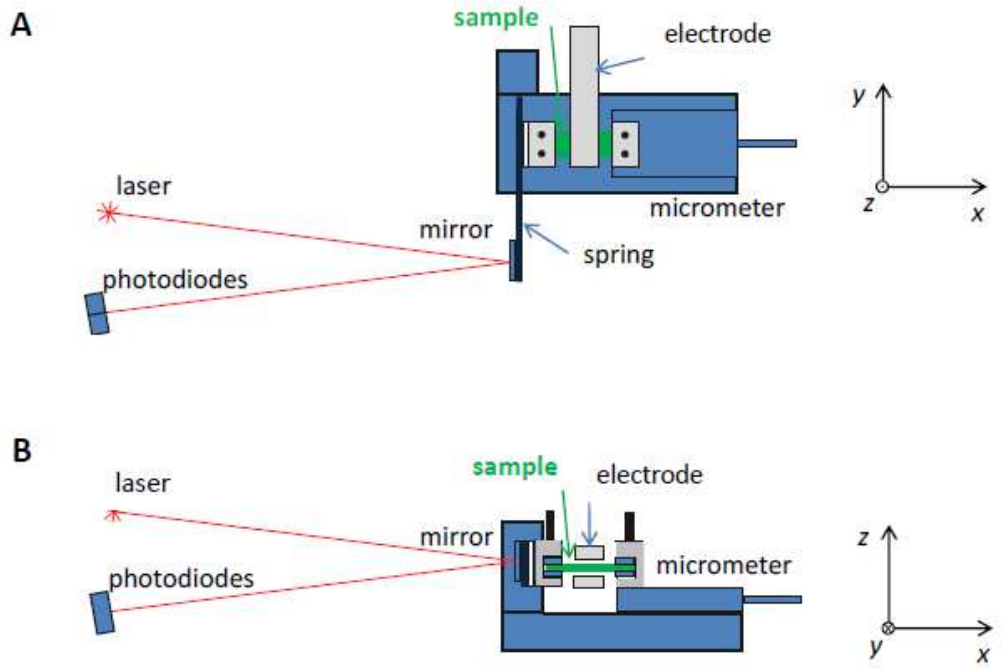

Figure 2. Schematic of the setup used to measure the converse piezoelectric effect, (A) top view and (B) side view.

The converse piezoelectric coefficient d_{31} was calculated, in the used setup configuration, as:

$$d_{31} = 2.1 \cdot 10^4 \frac{D\varepsilon_s}{l_e} \frac{V_{out,RMS}}{F_{sim}} \quad (1)$$

where D is the spacing between electrodes, l_e the electrode size along x, $V_{out,RMS}$ the vibration amplitude output of the apparatus, and

$$\varepsilon_S = \varepsilon_d - \frac{D_d}{D}(\varepsilon_d - 1) \quad (2)$$

where ε_d is the effective dielectric constant of the composite and D_d the strip thickness. ε_d was calculated with the model from Bhimasankaram and co-workers [30, 31] as:

$$\varepsilon_d = \frac{\varepsilon_P(1-q) + \varepsilon_{BT} q[3\varepsilon_P/(\varepsilon_{BT}+2\varepsilon_P)][1+3q(\varepsilon_{BT}-\varepsilon_P)/(\varepsilon_{BT}+2\varepsilon_P)]}{(1-q) + q[3\varepsilon_P/(\varepsilon_{BT}+2\varepsilon_P)][1+3q(\varepsilon_{BT}-\varepsilon_P)/(\varepsilon_{BT}+2\varepsilon_P)]} \quad (3)$$

with ε_P the dielectric constant of the polymer, ε_{BT} that one of the BTNPs, and q the volume fraction of the BTNPs. Values used in the present experiment were D = 1 mm, l_e = 6.5 mm, ε_P = 12, ε_{BT} = 1250, ρ_P = 1.78 g·cm^{-3}, ρ_{BT} = 6.02 g·cm^{-3}. To obtain an effective sample thickness D_d of the fiber mesh samples, weighing by an analytic scale was performed to determine the effective volume of fibers, and the effective thickness was obtained by dividing by the sample area. The value of the calibration factor in Eq. (1) depends on various characteristic of the setup in the used configuration, as optical lever length and photodiode sensitivity.

The F_{sim} value in Eq. (1) deserves special discussion. In the case of a rigid sample, such factor can be approximated by the quality factor Q of the mechanical resonance of the measurement spring. However, for soft samples like the ones here characterized, such approximation fails, making this kind of measurements a challenging task. We have faced this problem by adopting a mechanical model of the system of springs, composed by the measurement spring and the sample. To such purpose, a *Mathematica*™ script was developed. Since the spring constant of the fiber mesh strips (k_s of the order of 1-2 kN·m^{-1}) was much lower than the one of the measurement spring (k_b = 26 kN·m^{-1}), it was possible to measure such spring constant by the same setup used for the piezoelectric measurements, although with a high uncertainty (30%). Then such values were used for calculating the scaling factors F_{sim} by our model, to be inserted in Eq. (1) obtaining the best estimate for piezoelectric coefficients. For low spring constants, it turns out that the same uncertainty on the spring constant is translated to the value of F_{sim}.

Finally, the direct piezoelectric coefficient g_{31} was calculated as:

$$g_{31} = \frac{d_{31}}{\varepsilon_0 \varepsilon_d} \tag{4}$$

being $\varepsilon_0 = 8.82 \cdot 10^{-12}$ F/m the dielectric constant of vacuum.

A PVDF uniaxially-poled metallized film (from Goodfellow Cambridge Ltd. Huntingdon, UK) was used as a positive control, whereas poly(ethylene oxide terephthalate)/poly(butylene terephthalate) (PEOT/PBT) randomly electrospun fiber mesh was used as a negative control for the experiment [32]. Measurements on piezoelectric fiber strips were repeated at least three times. Experimental error of piezoelectric coefficients resulted about 30%.

2.9 *In vitro* culture of inner ear epithelial cells with BTNP/PVDF fibers

This biomaterial device is designed for intracochlear application (e.g., through the *scala tympani*), which is a delicate microenvironment. In future clinical applications it will be important to preserve residual hair loss. The OC-k3 cell line was used as a model of hair cells to assess cytocompatibility of the electrospun BTNP/PVDF fibers. OC-k3 are epithelial cells isolated from the organ of Corti of a transgenic mouse (ImmortomouseTM H-2Kb-tsA58). The fibers (dimensions 1 cm × 0.5 cm) were placed on coverslips and sterilized with absolute ethanol overnight (BioOptica, Milan, Italy). The different composition samples (n = 2) were placed in 6 well plates, let dry under the biohood and rinsed with sterile saline before usage. OC-k3 cells were seeded at $1.5 \cdot 10^5$ cells/fibers and cultured in incubator under non-standard conditions (33°C, 95% relative humidity, 10% CO_2/90% air environment), using Dulbecco's Modified Eagle Medium (DMEM Gibco BRL, Gaithersburg, MD, USA), supplemented with 10% fetal bovine serum (Gibco), L-Glutamine 2 mM (Gibco), Pen-Strep 1% (Gibco) and 50 U/ml of recombinant mouse γ-interferon (IFN, Genzyme, Cambridge, MA, USA). After 72 h, the samples were washed twice with PBS 1× and then fixed with Gliofixx for 30 min at room temperature. The samples were subsequently washed with PBS 1× and treated with 0.1% Tween/PBS (Sigma-Aldrich) 1× for 10 min and the surfactant solution was then removed by PBS 1× wash. The visualization of nuclear morphology was achieved by staining the samples with 2 mg/ml 4,6-diamidino-2-phenylindole (DAPI, Sigma), which selectively stains DNA. The slides were mounted with DABCO glycerol and examined under a fluorescence microscope equipped with the appropriate filters (Nikon Eclipse TS100, Melville, USA).

2.10 Dynamic *in vitro* culture of neural cells on BTNP/PVDF fibers

As a proof of concept, the 15% BTNP/PVDF fibers were cultured for 1 week with SHSY-5Y cells (CRL-2266 ATCC, LGC Standards, Milan, Italy) inside a bioreactor (dynamic culture system) and compared to traditional culture method (static culture system) (n = 1). The bioreactor used in this study is able to impart a bidirectional cyclic bending deformation, and was considered for this preliminary study as a basic biomimetic stimulation of cochlear mechanics. The bioreactor is a patented custom-made apparatus that allows the vertical oscillatory motion of the cell/biomaterial samples in a sterile disposable tube at a defined frequency, using a double-ring Teflon frame as a sample holder (PCT/IB2014/064593). SHSY-5Y is a human neuroblastoma-derived cell line known to be dopamine β hydroxylase active and express neural markers, thus representing a valuable model of human neural cells for *in vitro* experiments. Cryopreserved cells were defrosted and expanded in growth medium composed of 1:1 (v/v) Eagle's Minimum Essential Medium (E-MEM; ATCC) and F12 Medium (Sigma-Aldrich), added with 10% heat inactivated fetal bovine serum

(Invitrogen, Carlsbald, CA, USA), antibiotics (100 IU/ml penicillin + 100 mg/ml streptomycin; Sigma-Aldrich) and 2.5 μg/ml antimycotic (Diflucan, Pfizer-Italia, Latina, Italy). The 15/85 BTNP/PVDF fiber ribbons (size 2.2 × 0.5 cm^2), previously clipped to the sample holders, were placed inside 6 well plates and sterilized in absolute ethanol (BioOptica) overnight, followed by 3 rinses, 10 min each, in sterile saline with 3× antibiotics/antimycotic. The cells were seeded onto the fiber ribbons, previously coated with a 2% (w/v) sterile aqueous solution of gelatin (75 Bloom, type B from bovine skin, Sigma-Aldrich), at a density of $1.5 \cdot 10^6$ cells/scaffold using the plasma clot method [33]. Specifically, 50 μl of pooled human plasma were added with 20 μl calcium chloride solution (Bioindustria Farmaceutici s.r.l., Labaro, RM, Italy) at 7 mM final concentration, to generate a fibrin clot which embedded the cells and the scaffold, thus preventing cell dropping. After performing 7 days static culture for both samples using a neuro-differentiating medium composed of growth medium added with 10 μM all-trans retinoic acid (ATRA, Sigma-Aldrich), one was moved into the bioreactor, and the culture was continued in the same conditions for 7 days. The bioreactor was set to alternate 15 min periods of 0.23 Hz movement and rest. The culture was performed in an incubator under standard condition, namely, 37 °C, 95% relative humidity, and 5% CO_2/95% air environment.

At the endpoint, cell viability and morphology were observed under fluorescence with Calcein-AM dye (LIVE/DEAD® cell viability kit, Life Technologies). Briefly, at the endpoint, the bioreactor was stopped and the sample put back to a 6 well plate, the culture medium was replaced with a staining solution consisting of sterile phosphate buffered saline (PBS, Sigma-Aldrich) added with 0.5 $\mu l \cdot ml^{-1}$ Calcein AM. After 30 min incubation in the dark at 37°C, the samples were observed under an inverted light microscope (Eclipse TI, Nikon, Tokyo, Japan) equipped for fluorescence analysis and FITC filter. Calcein AM dye stains in green the cells that show intracellular esterase activity, i.e., live cells. Dynamically and statically cultured samples were imaged at 5× and 10× magnifications taking representative pictures for each sample with an exposure time of 100 ms.

2.11 Statistical analysis

Data sets of the fiber diameter obtained for each tested condition were screened by one-way ANOVA and a Tukey test was used for post hoc analysis; significance was defined at $p < 0.05$. Results are presented as mean values ± standard deviation (SD).

3 Results and Discussion

SNHL is a pathology that affects the inner ear, leading to a dismal deafness condition. It is determined by damages of hair cells, a sensory epithelium of the cochlea located in the organ of Corti, which do not properly perform signal transduction, from mechanic (fluid waves) to electric (depolarisation of spiral ganglion neurons), while the nerve is still functioning. Piezoelectric materials possess the unique property of generating electric charges via self-polarization under mechanical force application, thus acting as mechano-electrical transducers that can mimic the function of the cochlear sensory epithelium [17]. By inserting a silicon/PVDF membrane in the *scala tympani*, the outputs obtained in an animal model resulted in the ten-of-μV order of magnitude, namely, an insufficient sensitivity to depolarize the underlying nerve of at least 10^4 [17]. Reaching an effective sensitivity is indeed very challenging. The aim of this study was to smartly combine topographical, chemical and physical cues in a single platform designed for cochlear stimulation by using piezoelectric nanocomposites with attractive features for neural cells. Owing to their superb tailorability, multifunctional piezoelectric transducers aided by tissue engineering could move a step forward the current piezoelectric CIs.

3.1 Production, morphology and topography of BTNP/PVDF fibers

The first goal of this research was the production of ceramic/polymer composite fibers to increase the material piezoelectricity. Ceramic/polymer composites can increase the piezoelectric coefficients of transducers [10-12]. Moreover, nanostructured materials, such as aligned ultrafine fibers, can modulate neural cell activity by promoting cell/interface contact and therefore increasing the device performance [34]. For these reasons, in this study we designed piezoelectric composites in form of ultrafine fibers. Specifically, BTNP/PVDF fibers were produced via electrospinning with BTNP weight ratios ranging in 0%-20%. The production of random-to-aligned electrospun fibers was also performed by collecting the polymeric jet onto a rotating disk with low-to-high tangential velocity (V_t). By changing the V_t of the rotating disk collector, different fiber diameter and alignment were obtained and different mesh morphologies were observed. The morphology of the obtained meshes was characterized and the dispersion of BTNPs inside the PVDF fibers was analyzed. The processing parameters and the different electrospun mesh compositions are summarized in **Table 1**.

Fiber morphology, microstructure and layout were evaluated using SEM. The obtained fiber diameters decreased with the increase of the collector V_t, although differences between datasets were not statistically significant (**Table 1**). Fiber diameter varied ranging from 500 ± 125 nm (V_t = 3.7 m·s^{-1}) to 395 ± 119 nm (V_t = 22.0 m·s^{-1}). Using BTNPs as fillers of PVDF fibers did not induce

significant changes over the fiber diameter, which ranged from 506 ± 141 nm (V_t = 3.7 m·s^{-1}, for BTNP/PVDF 10/90) to 385 ± 111 nm (V_t = 22.0 m·s^{-1}, for BTNP/PVDF 20/80). An increase of V_t also induced a reduction (not statistically significant) of the fiber diameter obtained for the composite fibers. The average fiber diameter was in accordance with different previously reported studies [29, 35]. The co-solvent system used (DMF and acetone) was selected according to previously reported works [29, 36, 37]. Basing on a study of Yee *et al.* [37], which reported that an increase of DMF/acetone ratio induced a decrease in fiber diameter and an increase of beads present on the electrospun mesh, the 1:1 DMF/acetone ratio was selected for conducting our experiments.

Table 1 – Fabrication parameters and obtained fiber diameters for the different meshes produced.

BTNP/PVDF weight ratio (% w/w)	**PVDF concentration in the co-solvent system (% w/v)**	**Collector rotation (rpm)**	**Tangential velocity (m·s^{-1})**	**d1/d2 (cm)**	**Voltage (kV)**	**Feed rate (ml·h^{-1})**	**Fiber diameter (nm)**
0/100	20	500	3.7	15/1	20	1	500 ± 125
	20	1500	11.0	15/1	20	1	473 ± 127
	20	2000	14.7	15/1	20	1	428 ± 97
	20	3000	22.0	15/1	20	1	395 ± 119
10/90	20	500	3.7	15/1	20	1	506 ± 141
	20	1500	11.0	15/1	20	1	439 ± 159
	20	2000	14.7	15/1	20	1	420 ± 141
	20	3000	22.0	15/1	20	1	405 ± 142
15/85	20	500	3.7	15/1	20	1	499 ± 147
	20	3000	22.0	15/1	20	1	480 ± 162
20/80	20	500	3.7	15/1	20	1	412 ± 122
	20	3000	22.0	15/1	20	1	385 ± 111

The flow rate selected for the experiments was 1 ml·h^{-1} and was kept constant for all the experiments. The morphologic effect played by V_t over fiber morphology and arrangement for BTNP/PVDF 0/100 and 10/90 w/w electrospun fibers is displayed in **Figure 3**, which corroborates the results summarized in Table 1. From a qualitative evaluation, higher V_t seemed to favor fiber alignment and bead reduction over all the BTNP/PVDF compositions (**Figure 4**). The presence of BTNPs inside the fibers was observed under STEM. Increasing BTNP loading onto the electrospun fibers, induced and higher number of beads present on the electrospun meshes. As an example, the STEM analysis of BTNP/PVDF 10/90 is reported in **Figure 5**. BTNPs were quite uniformly

distributed inside the PVDF fiber matrix (**Figure 5 A, B**), although, in some regions, nanoparticle aggregates were observed inducing the formation of beads (**Figure 5 C, D**).

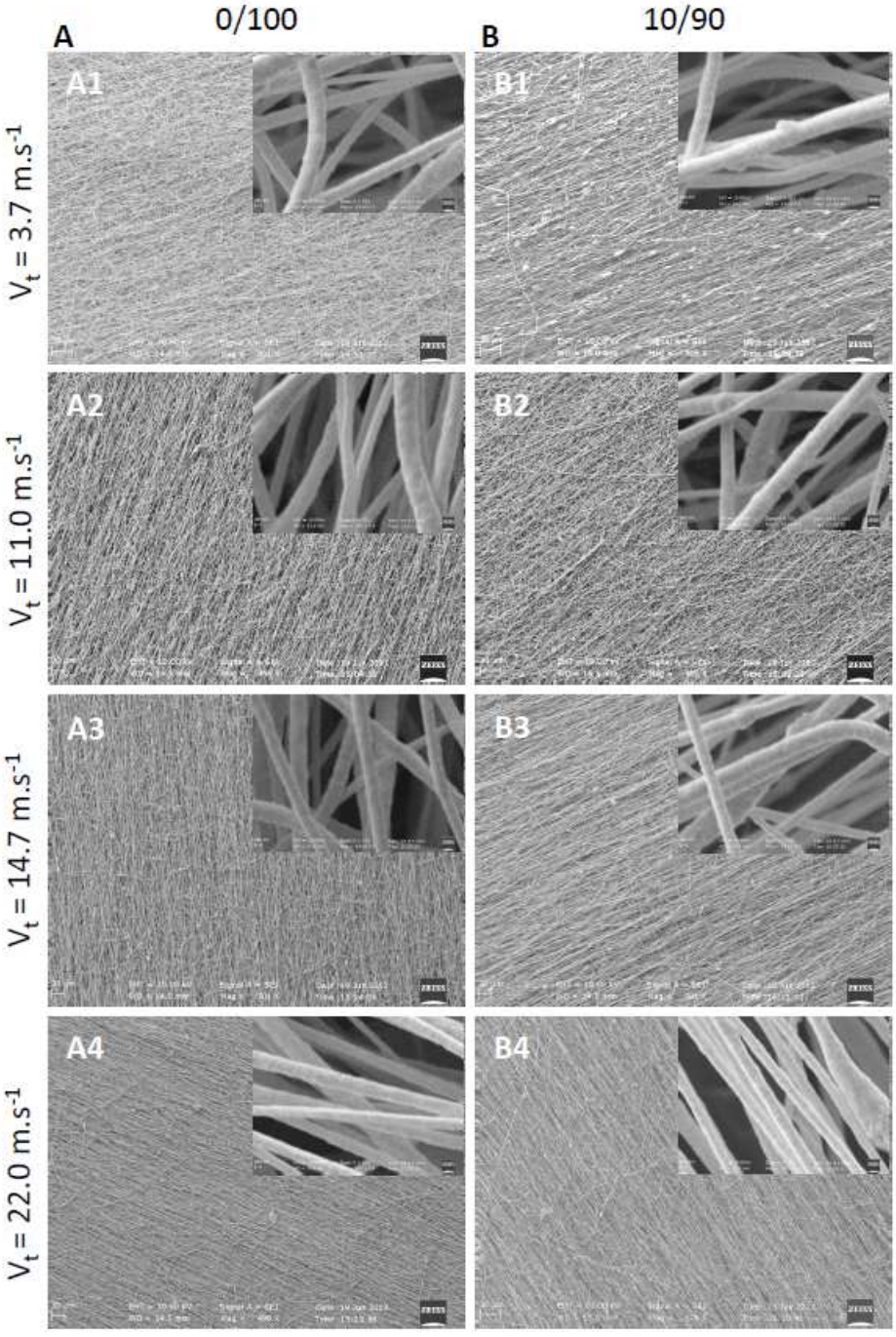

Figure 3 – Morphology of BTNP/PVDF electrospun fibers collected on a rotating disk at different tangential velocities in the range of 3.7 to 22.0 m·s^{-1}; (A) 0/100 and (B) 10/90 w/w compositions.

Scanning probe microscopes are a family of tools used to make images of nanoscale surfaces and structures, including atoms. They use a physical probe to scan back and forth over the surface of a sample. By removing the fiber mesh from the aluminum substrate on which the mesh was deposited by electrospinning, only the fibers adhering directly to the substrate were left.

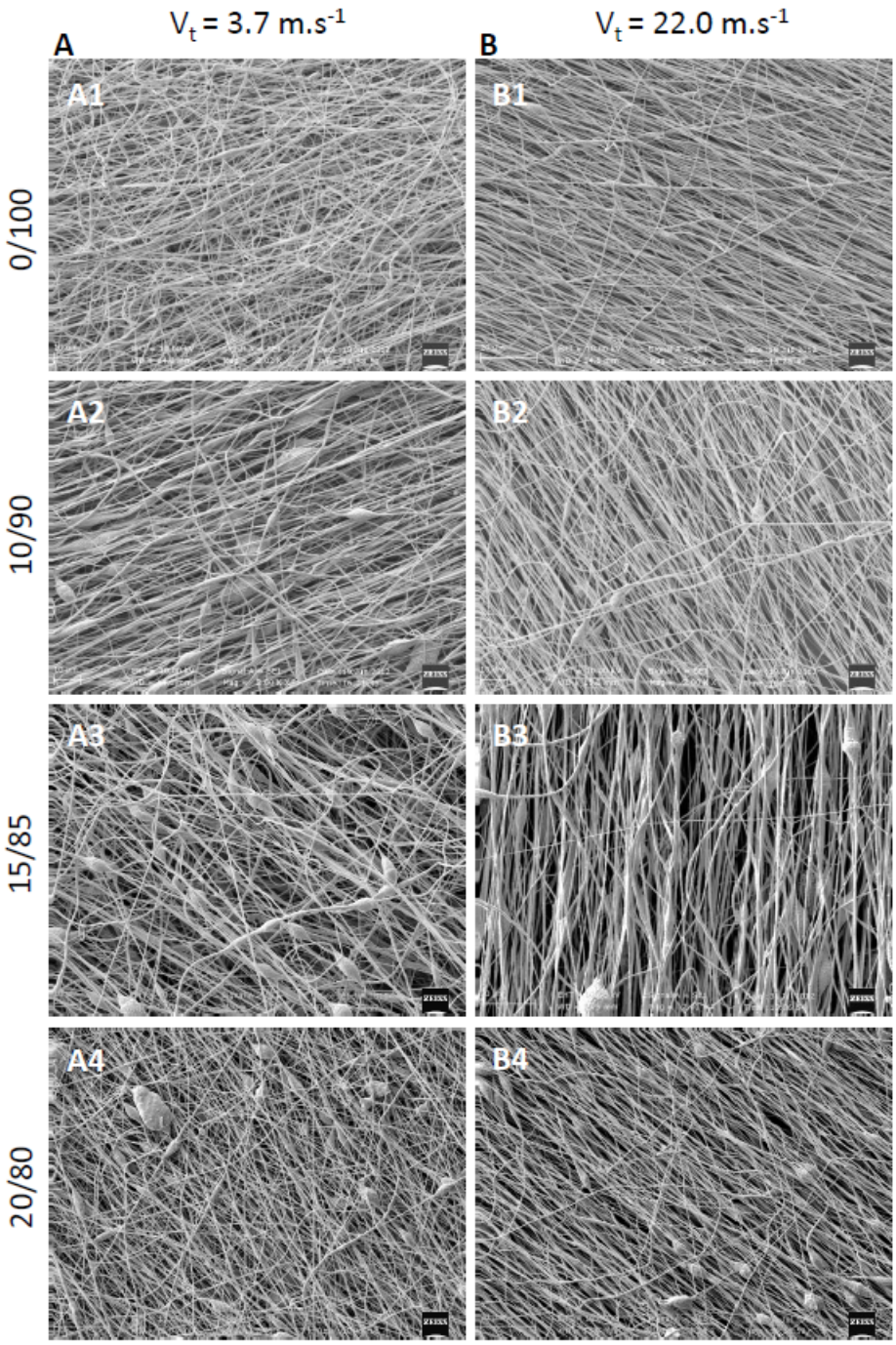

Figure 4 – Morphology of BTNP/PVDF electrospun fibers of different weight compositions, in the range of 0/100 to 20/80, collected on a rotating disk at low and high tangential velocity; (A) 3.7 m·s^{-1}and (B) 22.0 m·s^{-1}.

Such fibers were supported strongly enough to be imaged by AFM. A typical image is shown in **Figure 6 A**. Defects visible on the straight polymer fibers can be ascribed to some of the incorporated BTNPs emerging from the fiber surface. While the best known scanning probe microscopies work in a similar configuration, SNOM adopts a different approach to reach the surface. It uses a vertical tuning-fork tip approaching from the top to down and exploiting the so-called shear force system. This gives a clear advantage when scanning a material that is

characterized by irregular very soft compliance under the scanning probe tip. SNOM analysis highlighted that BTNP/PVDF fibers showed cylinder symmetry and surface nanowrinkles having nearly 40 nm for height (h) and width (w). The average h/w ratio was 0.94 ± 0.26 (**Figure 6 B, C**). Surface topography is a prominent feature in tissue engineering that can influence cell adhesion and function, including immune cell response [38]. From this extensive analysis, it was concluded that up to the BTNP/PVDF weight composition 20/80 and within the V_t range investigated, no significant changes in fiber diameter, morphology and topography could be observed. BTNP aggregation was imaged more frequently at lower V_t and higher BTNP content.

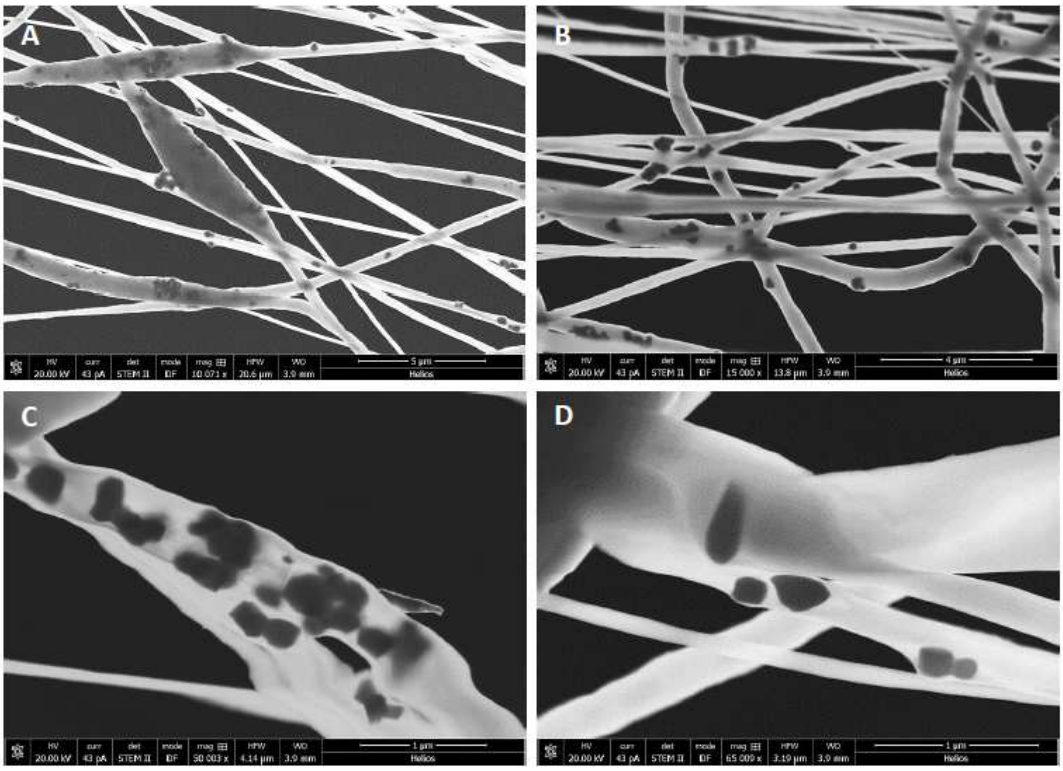

Figure 5 – STEM micrographs of BTNP/PVDF 10/90 electrospun fibers obtained with a collector tangential velocity of 3.7 $m \cdot s^{-1}$ at different magnifications in the range of 10,000× to 65,000×. (A, B) dispersion of BTNPs inside the electrospun fibers; (A) beads induced by the presence of BTNP aggregates; (C) BTNP aggregates inside an electrospun fiber; and (D) BTNP dispersed inside an electrospun fiber.

3.2 Alignment of BTNP/PVDF fibers

The second goal of this study was the fabrication of BTNP/PVDF composite fibers in form of fiber meshes aligned along the longitudinal axis. It has been observed that biomaterial scaffolds act as a microenvironment at cellular level by offering topographic and physical cues, as well as three-dimensional architectures, which the cells can interact through functional and morphological responses [39]. Certain scaffold topographies may be most instructive to specific cell types by mimicking some features of their native extracellular matrix. In particular, in neural tissue

engineering, the anisotropic properties of aligned nanofibers were best suitable to provide spatial guidance for neurite outgrowth [34].

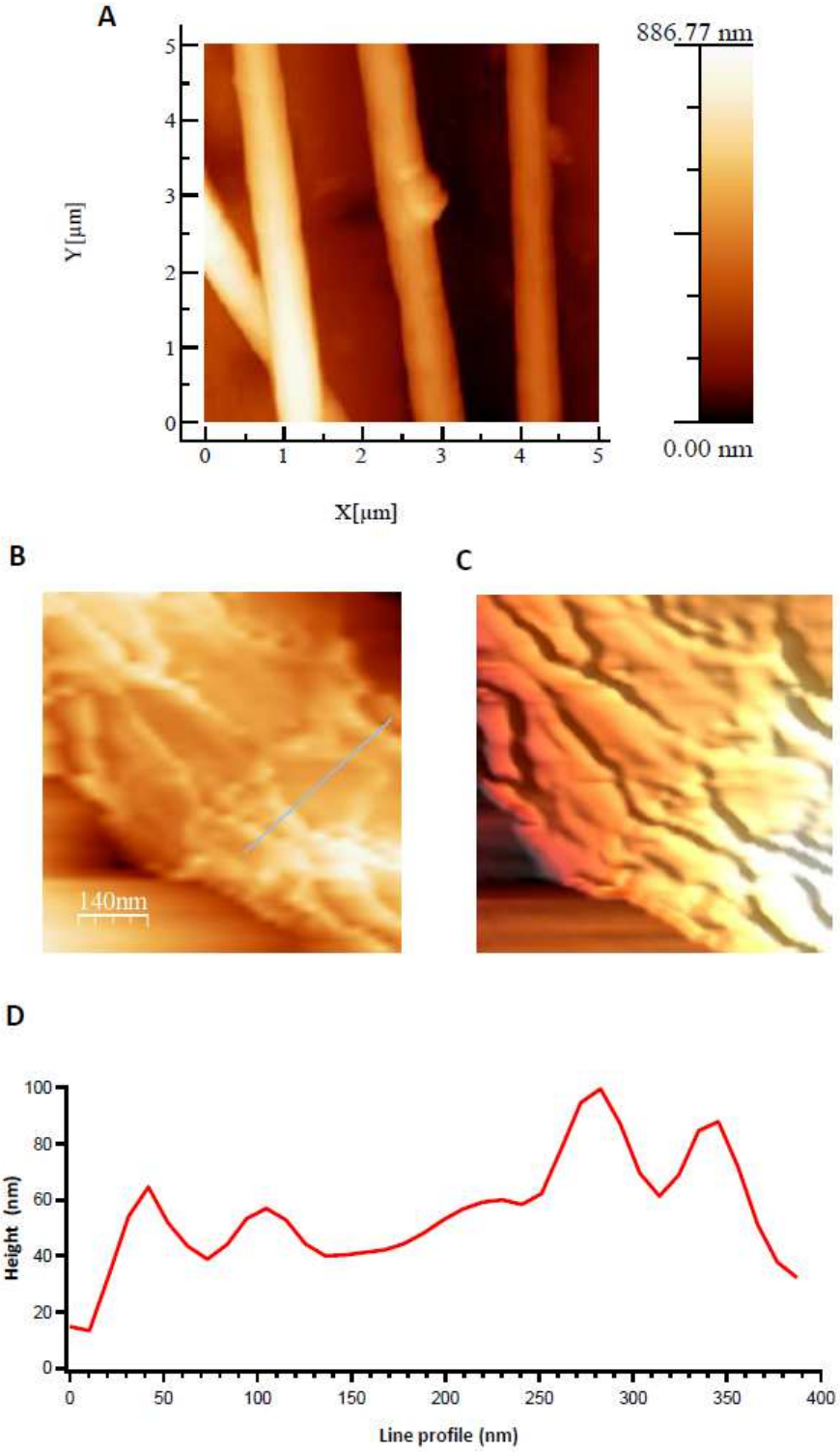

Figure 6 – Topographical analysis of BTNP/PVDF fibers. (A) A representative tapping mode AFM micrograph showing the surface topography of the fibers and a BTNP emerging from the polymer; (B-C) Representative results of SNOM analysis: (B) Surface topography of the fiber showing nanowrinkles, (C) Pseudo 3D reconstruction, and (D) fiber profile along the blue line in (B).

The obtainment of aligned fibers produced via electrospinning is possible by changing the electrical field configuration with the aid of customized spinneret apparatus and/or by collector system [40]. The most common approaches used are rotating cylinder [41-43] or disk [44, 45] as collectors to mechanical winding the fibers, or by customized static or rotating [46] pattern collectors. Fiber alignment was evaluated with two dimensional FFT according to the method of Ayres *et al.* [47]. FFT converts mathematically the information of an image into a frequency domain and subsequently the pixel intensity is quantified over the spatial domain. With the increment of fiber alignment, a narrower or a higher peak of the two dimensional FFT plots was observed (**Figure 7**). The fiber alignment increased proportionally to the tangential velocity of the collector. For a low tangential velocity (3.7 $m \cdot s^{-1}$), the fibers were randomly assembled, in a similar fashion to the arrangements generally obtained on a static collector (**Figures 3 A1-B1** and **4 A**). An increase of the tangential velocity of the collector to 22.0 $m \cdot s^{-1}$ improved the uniaxial fiber disposition of the electrospun meshes, although some random fiber could still be observed. It should be noted that a few random fibers can be useful to keep together the fiber bundle upon manipulation. On the microscale, fiber alignment could also be directly visualized by tapping-mode AFM (**Figure 6 A**). Fiber alignment was consistent to expectations and in agreement with SEM characterizations.

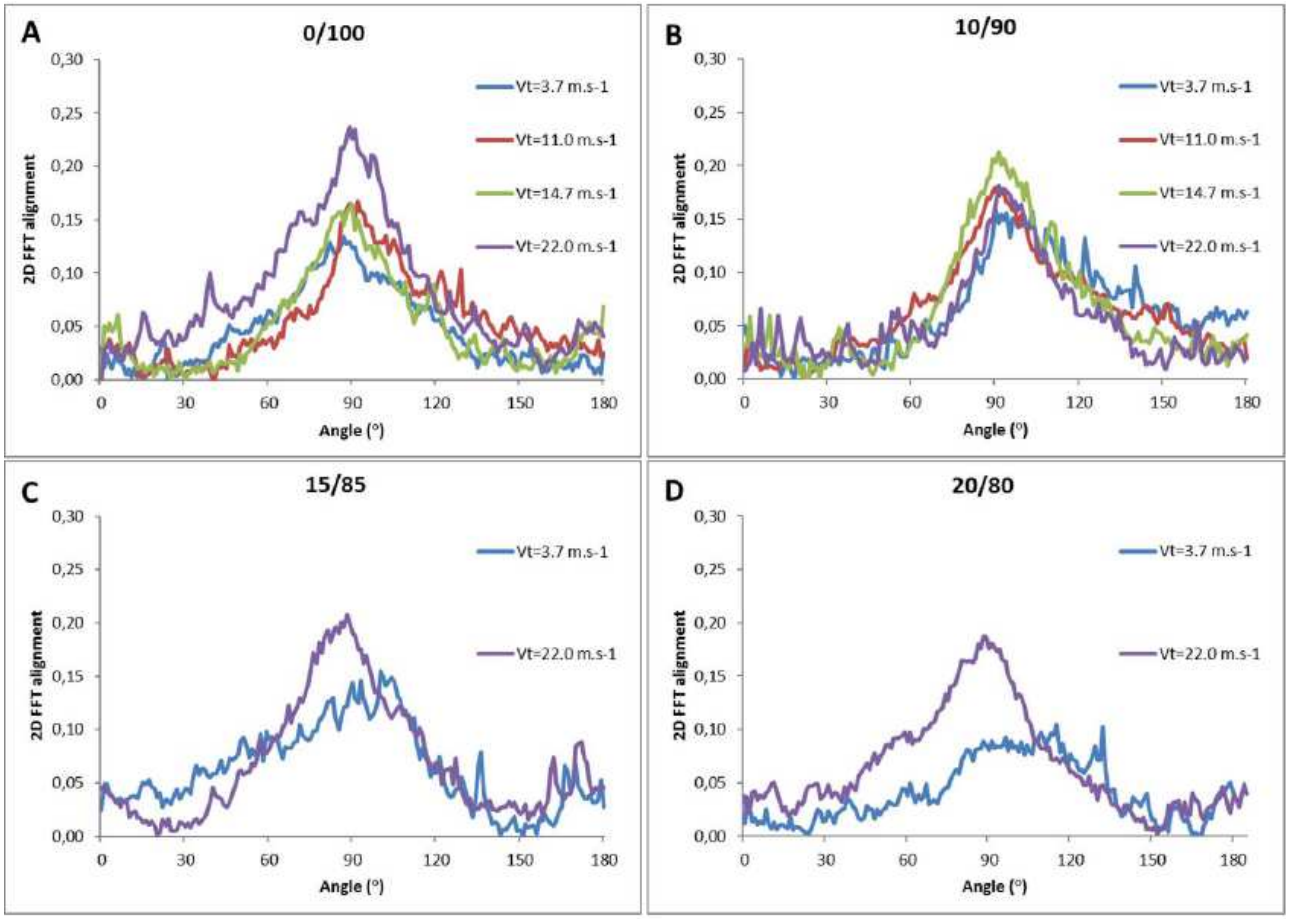

Figure 7 – Two-dimensional FFT plots of fibers collected at different tangential velocities for the following BTNP/PVDF weight compositions: (A) 0/100; (B) 10/90; (C) 15/85; and (D) 20/80.

3.3 Piezoelectric and mechanical properties of BTNP/PVDF fibers

The third goal of this study was to assess the piezoelectric properties of BTNP/PVDF fibers. XRD and ATR-FTIR were used to evaluate the presence of the piezoelectric crystallographic phases β in the produced materials, as shown in **Figure 8**. Specifically, in BTNP/PVDF fibers, XRD showed the occurrence of the 2θ = 19° peak of the PVDF β phase, together with the two peaks at 2θ = 44.85° and 45.38° proper of the $BaTiO_3$ β phase (**Figure 8 A,B**). ATR-FTIR was used to assess the proportion between the piezoelectric β and the non-piezoelectric α phases in raw versus electrospun PVDF (**Figure 8 C**).

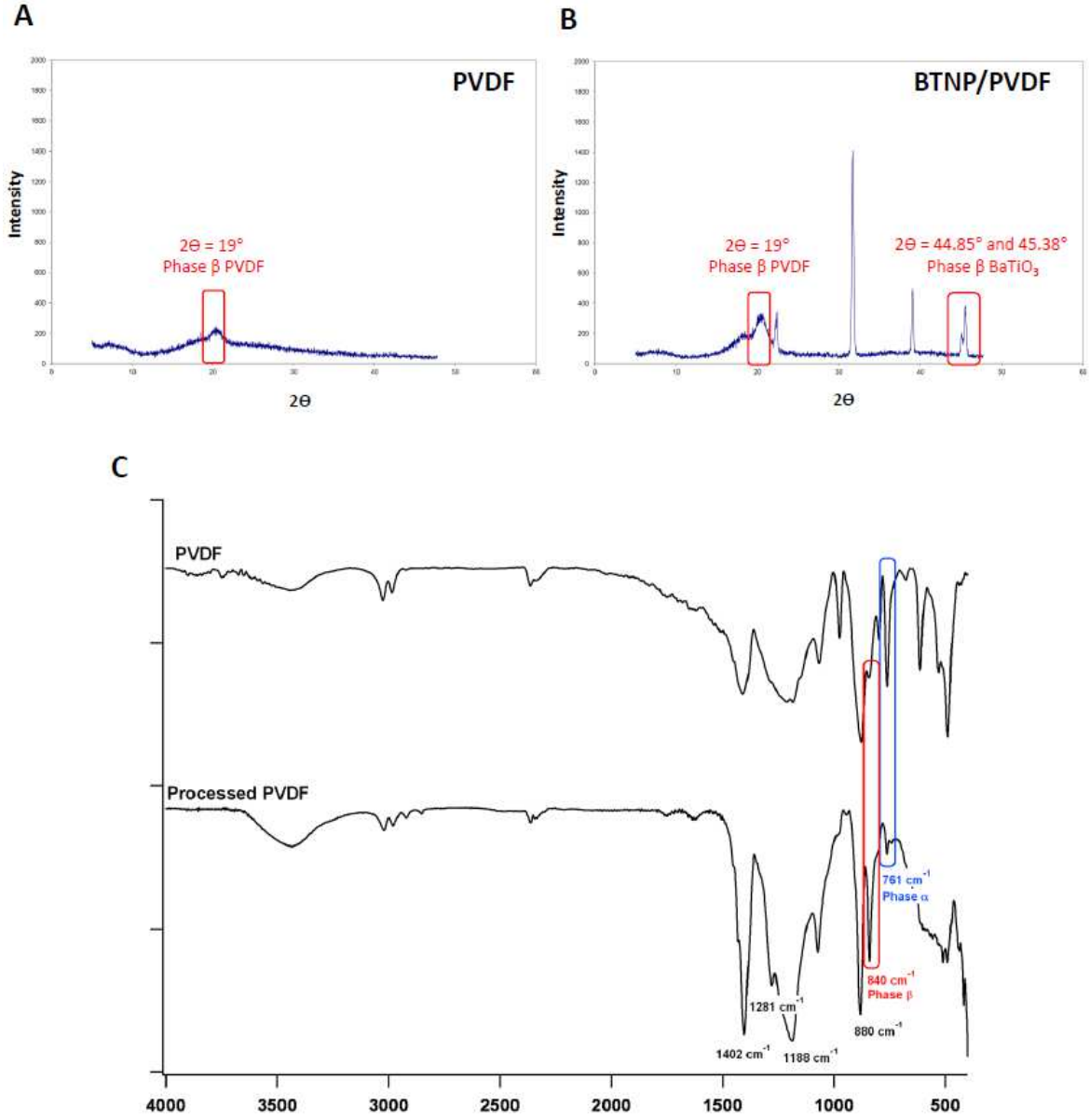

Figure 8 – Characterization of crystalline phases. (A, B) XRD analysis showing the 2θ peaks in BTNP/PVDF fibers corresponding to the piezoelectric β phases of PVDF and $BaTiO_3$: (A) 0/100 and (B) 20/80 weight compositions. (C) ATR-FTIR analysis showing the peak intensity of the non-piezoelectric α phase and the piezoelectric β phase in the raw PVDF and the electrospun PVDF fibers.

In particular, the intensities of the peaks corresponding to β and α phases were modified by the electrospinning process and gave rise to an enhancement of the 840 cm^{-1} peak, which is a fingerprint of β phase, to the detriment of the 761 cm^{-1} peak, which is used, among others, for α phase identification in PVDF. This result confirms that the electrospinning processing induced a poling effect on the fibers by increasing their piezoelectric properties.

Electrospun polymer fibers are obtained by stretching a polymer solution via electrostatic forces. Such a stretching may induce an extended chain conformation, in a different fashion from conventional solution or melt fiber deposition, which can ultimately affect the mechanical properties of the fibers.

Although some methods have been reported to measure the mechanical properties of single fibers and thick fiber meshes produced by electrospinning [48], the measurement of thin fiber meshes may be challenging owing to the difficulties in their manipulation under conventional equipment. The electrospun fiber meshes designed for this application were very thin to be inserted in the *scala tympani*. Consequently, they resulted delicate at handling and therefore an *in situ* tensile test performed under ESEM was considered a suitable method to provide this study with a basic mechanical characterization. Moreover, this equipment allowed the morphological behavior of the ultrafine fibers to be observed during the test, thus resulting a simple method to simulate their mechanical response. *In situ* tensile ESEM analysis showed that under an applied force ranging in 0.06 – 0.145 N, those fiber bundles aligned in the force direction supported the tension of the structure, up to an elongation of 4.81 mm. Basing on the test setup, this elongation corresponded to a strain percent of 48.1%, which is suggestive of a viscoelastic-plastic behavior (**Figure 9 A**). Since the actual cross-section area of the fiber ribbon is unknown, in these experimental conditions, the tension and therefore the Young's modulus cannot be evaluated. A dedicated study would be necessary to properly evaluate the real cross section area. The results of tensile test was finally reported as force versus strain. Owing to sample traveling upon elongation (maximum travel 5.457 mm), the images captured by the microscope over time did not belong to identical sample portions and were only representative of the mesh, showing absence of detectable morphological alterations (**Figure 9 A**). The environment of application of these materials is the basilar membrane of the cochlea, which is known to vary in width, thickness and elasticity as it curls from the oval window out to the helicotrema [49]. To further investigate the mechanical behavior of these fibers, DMTA was performed at 37°C and in varying frequencies, namely 0.1 – 100 Hz (**Figure 9 B, C**). Also in this case, the obtained storage moduli E' must be considered qualitatively due to the rough estimation of the cross section area (**Figure 9 B**). Under these working conditions, the BTNP/PVDF fiber strips had moderately viscoelastic behavior. Loss tangent (tanδ) resulted limited and constant

over this frequency range, thus supporting the fact that the material had no predominant viscous effects (**Figure 9 C**). Finally, since tanδ is independent of the cross section area, these results have quantitative value. The hearing frequency range in humans is broadly considered from 250 – 8000 Hz, leading to the future necessity of performing higher frequency tests than those preliminarily reported here.

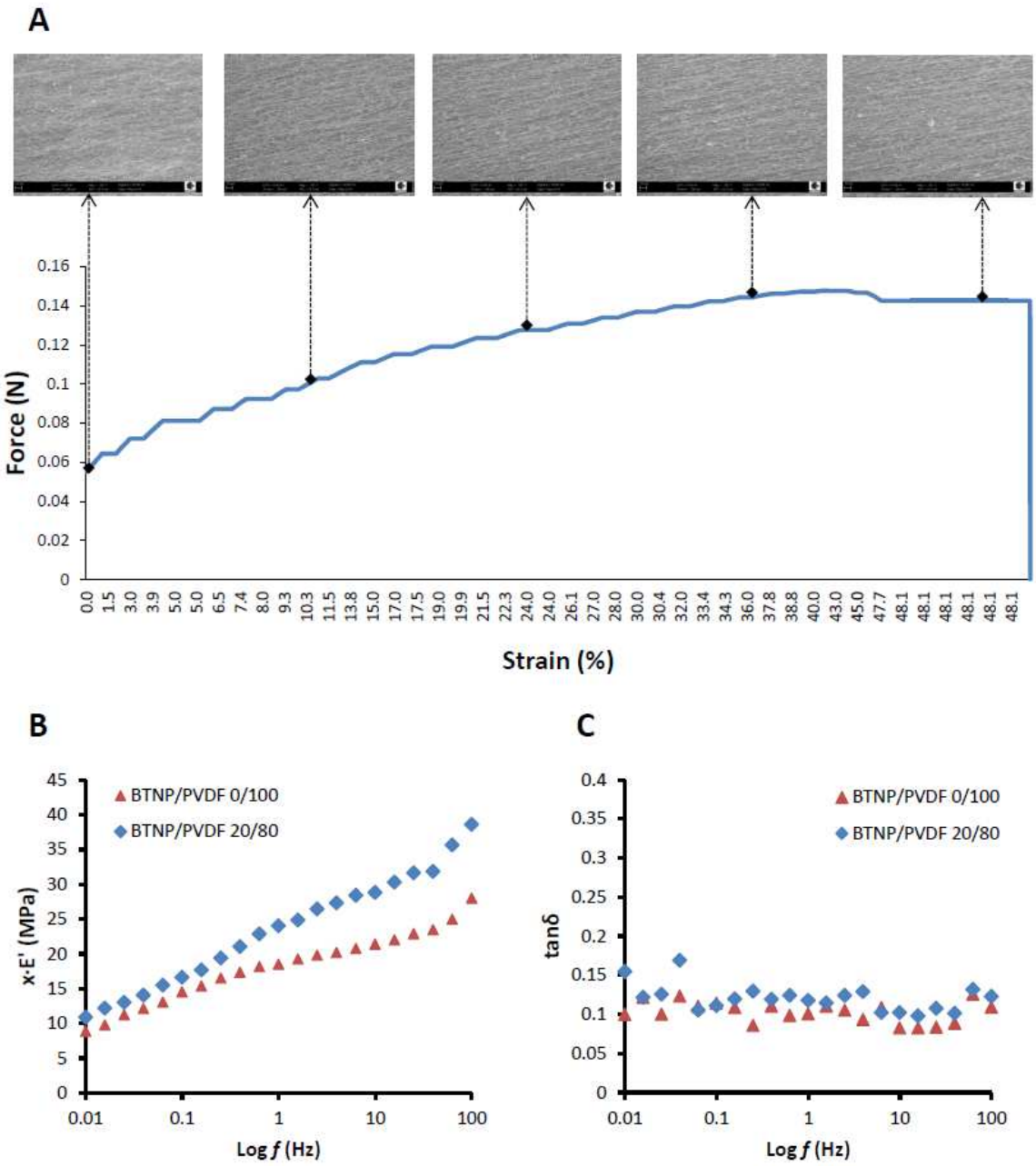

Figure 9 – Outcomes of mechanical tests performed on BTNP/PVDF fiber strips: (A) Results of *in situ* tensile ESEM test on BTNP/PVDF 20/80 w/w. The graph shows the qualitative trend of the applied force versus strain and in correspondence the morphology of the stretched fiber strips, until rupture. (B, C) Results of DMTA tests conducted at 37°C and 0.1 – 100 Hz on BTNP/PVDF 0/100 and 20/80 (w/w), showing in: (B) the qualitative trend of the storage modulus (E'); "x" is an unknown constant deriving from the rough estimation of the cross section area; and (C) the quantitative trend of tanδ. Results in (A, B) must be considered qualitative since the actual cross section areas could not properly determined in these samples.

A material to be adapted onto the basilar membrane and allow its proper vibration is required to be light and flexible, as the BTNP/PVDF fibers were found to be. However, additional studies will be necessary to define the mechanical interaction of these nanofibrous mats with the environment of application.

Finally, a dedicated setup was used to assess the piezoelectric properties of these fibers. The results of piezoelectric characterization are reported in **Table 2**.

Table 2 – Piezoelectric characterization of BTNP/PVDF fibers. Measurements are reported as mean ± standard deviation.

Sample	**PEOT/PBT (negative control)**	**PVDF Goodfellow (positive control)**	**BTNP/PVDF 0/100**	**BTNP/PVDF 10/90**	**BTNP/PVDF 15/85**	**BTNP/PVDF 20/80**
F	7 ± 2	55 ± 5	3 ± 1	4 ± 1	6 ± 2	4 ± 1
V_{out} (m·V_{RMS})	1.3 ± 0.3	80 ± 20	3 ± 1	5 ± 2	9 ± 3	10 ± 3
D_d (µm)	24	110	13.2	27.2	24.4	15.6
ε_r	4	12	12	13.3	14.1	15.0
ε_S	3.93	10.8	11.8	13.0	13.8	14.8
d_{31} (pm/V)	3 ± 1	60 ± 6	50 ± 20	60 ± 20	80 ± 20	130 ± 30
g_{31} (mV/N)	0.08 ± 0.02	0.6 ± 0.1	0.5 ± 0.2	0.5 ± 0.2	0.7 ± 0.2	1.0 ± 0.3

The trend of direct (g_{31}) and converse (d_{31}) piezoelectric coefficients is reported in **Figure 10**. The piezoelectric efficiency increased along with BTNPs content. Results for both positive and negative control materials are also reported in the same graph, validating the performance of this measurement technique. Moreover, it was noticed that piezoelectric performance increases with time during application of the excitation electric field needed to obtain piezoelectric strain. Such an electric field may tend to align ferroelectric domains during the measurements, providing as high values as the ones obtainable by poling at high temperature to obtain poled crystals. The reported values are the maximum ones obtained after at least 30 min of application of the excitation electric field.

3.4 Interaction of BTNP/PVDF fibers with inner ear epithelial and neural cells

The final goal of this research is to have preliminary evidence of cell interaction with the produced BTNP/PVDF fibers, namely to test their compatibility with cochlear epithelial cells and capability

of functional interaction with neural cells *in vitro*. These results serve as a supporting evidence of proper material design and fabrication, which can pave the way to subsequent in-depth biological studies. OC-k3 cells are epithelial cells from the mouse organ of Corti which can be used as an effective tool to study the ototoxicity [50].

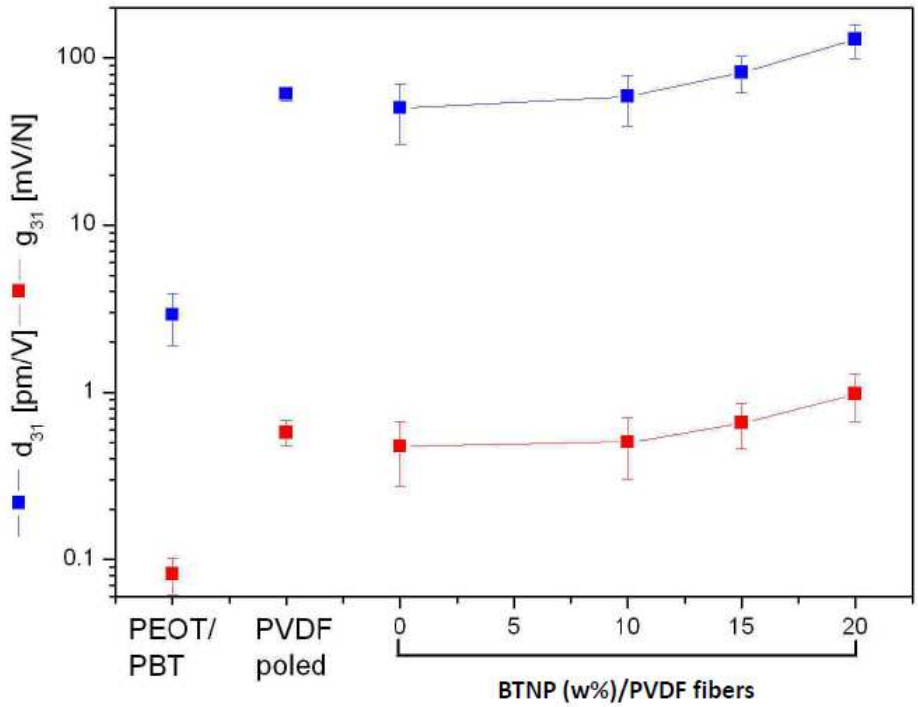

Figure 10 – Graph showing the values of the piezoelectric coefficients for the different materials tested: PEOT/PBT random fiber mesh (negative test), PVDF from Goodfellow (positive test), and the four different weight compositions of electrospun BTNP/PVDF fibers.

Indeed, one requirement of biomaterials to be inserted in the inner ear is the biocompatibility with such a delicate microenvironment, to preserve any residual hearing in deaf patients. In this study, OC-k3 cells were seeded into wells containing BTNP/PVDF fibers placed on coverslips. DAPI staining was used to assess presence of the cells and morphology of cell nuclei. A representative result of fluorescence microscopy observation, which was conducted on all BTNP/PVDF composition types, is reported in **Figure 11 A, B**. The OC-k3 cells showed intact nuclei in the areas surrounding the fibers, thus indicating that cytotoxic by-products or solvents were not released in the supernatant medium (**Figure 11 B**). The cells could also adhere to the fibers, as shown by DAPI stained nuclei in **Figure 11 A**, thus corroborating the material cytocompatibility, although the polymer autofluorescence in the blue channel prevented a detailed imaging of the cells.

Preliminary studies have demonstrated neural guidance by aligned fibrous scaffolds [34], and enhanced neurite sprout induced by ultrasound activated piezo-materials [21]. In the cochlear environment, the piezo-material is supposed to move under sound vibration, en bloc with the basilar membrane. Differently from the study conducted by Genchi *et al.* [21], in which the piezo-material

was cultured in static condition and irradiated with an ultrasound probe, in this study the piezo-material was placed inside a dynamic system moving at low frequency, therefore inducing a deformation. A bioreactor developed for tympanic membrane culture was adapted to this application to have preliminary evidence of function. Advanced *in vitro* culture systems that mimic physiological conditions, such as bioreactors, are very useful tools and ethically sustainable models for material and drug screening before *in vivo* applications. Under cyclic bending deformation for 1 week, SHSY-5Y cells were viable and developed longer neurites than those in static controls, thus suggesting an efficient cellular interaction with the piezoelectric substrate (**Figure 11 C, D**).

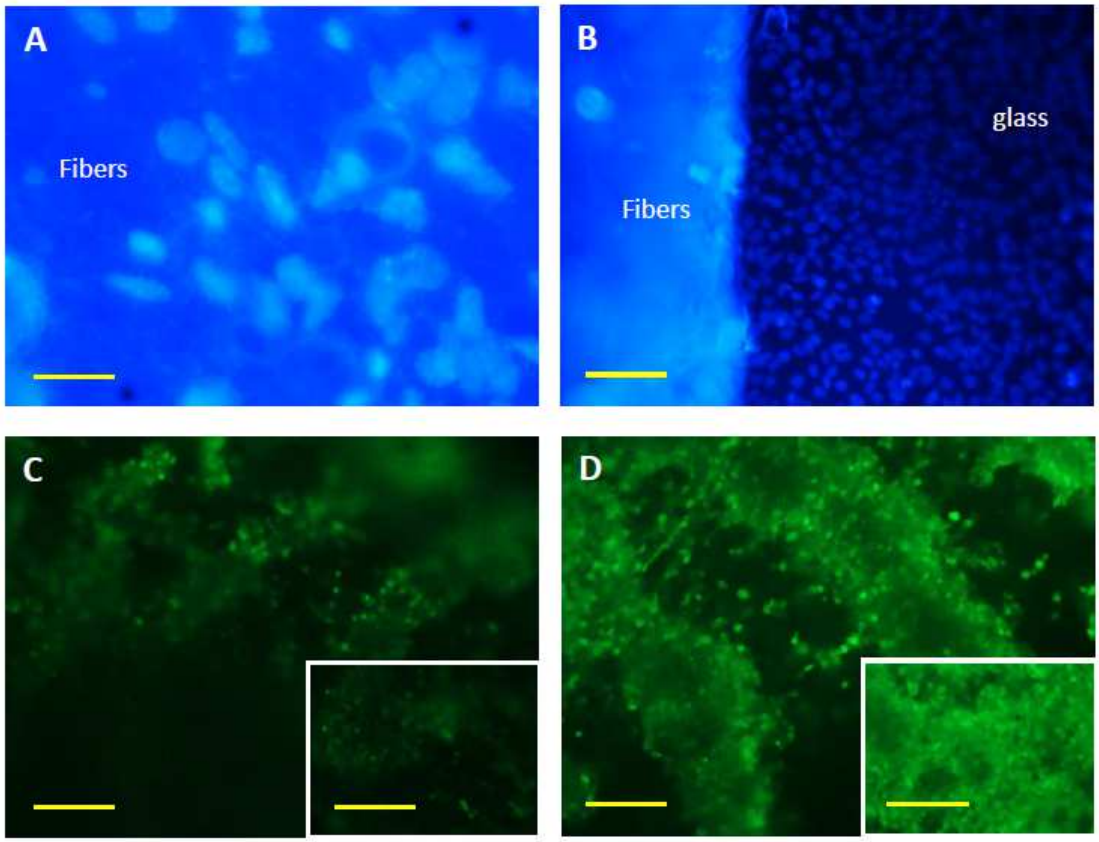

Figure 11 – Panel showing *in vitro* interaction of cells with BTNP/PVDF under fluorescence microscopy. (A, B) DAPI staining of OC-k3 inner ear epithelial cells cultured in presence of BTNP/PVDF 20/80 fibers: (A) Micrograph showing cell nuclei in the fibers; (B) Micrograph displaying many cell nuclei on the glass around the fibers. Scale bars are 10 µm. (C, D) Micrographs showing Calcein AM staining of SHSY-5Y neural-like cells cultured on BTNP/PVDF 15/85 fibers for 1 week under: (C) Conventional culture (static culture), and (D) Bioreactor culture (dynamic culture). Scale bars are 50 µm. Inserts in (C) and (D) highlight details of the samples at higher magnification. Scale bars are 25 µm.

Enhanced viability and function during dynamic culture have been observed in other applications and are invoked as a proof of reliability of biomimetic culture systems [32]. Further studies will be necessary to precisely demonstrate the hypothesis that BTNP/PVDF fibers can enhance the auditory performance in animal models and if their ability of attracting resident neurites of the spiral ganglion neurons will be confirmed *in vivo*.

4 Conclusions

Piezoelectric nanoceramic/polymer materials were designed and electrospun to manufacture thin meshes of BTNP/PVDF ultrafine fibers, as novel mechano-electrical transducers to restore cochlear function. Different fiber alignment degree was achieved by changing the rotation speed of the electrospinning disk collector. The fabricated BTNP/PVDF fibers showed an average diameter of 400 nm, nanowrinkled surface topography and enhanced PVDF piezoelectric β phase as a consequence of the processing method. The BTNP/PVDF fibers displayed an elastic behavior with moderate viscous dissipations up to 100 Hz frequency and the direct piezoelectric coefficient g_{31} averagely increased with BTNP weight percentage in BTNP/PVDF composites, namely, from 0.5 $mV \cdot N^{-1}$ (in 0/100 w/w) to 1.0 $mV \cdot N^{-1}$ (in 20/80 w/w). This result is predictive of an enhanced piezoresponse also along the *33* direction, and therefore of a higher sensitivity than that shown by plain PVDF films used so far in piezoelectric CIs. Finally, preliminary *in vitro* tests performed using inner ear epithelial cells and neural-like cells showed very good biocompatibility and confirmed that the nanofibrous material offered a suitable interface for neurites, displaying enhanced viability under physiology-simulated culture conditions. The obtained findings are highly suggestive that nanostructured piezoelectric materials will be able to improve the material performance by favoring the tissue/material interaction at targeted cellular level.

Acknowledgements

The authors greatly acknowledge the Italian Ministry of Health – Finalized Research Program 2011 for funding this study. Gianni Ciofani, IIT (Pontedera, PI, Italy) and Marco Paggi, IMT (Lucca, Italy) are kindly acknowledged for allowing the use of STEM and *in situ* tensile ESEM facilities, respectively. The authors thank Mr. Luca Panariello (University of Pisa, Italy) for his technical support to DMTA measurements.

References

[1] R. Fettiplace, C.M. Hackney, The sensory and motor roles of auditory hair cells, Nat Rev Neurosci 7(1) (2006) 19-29.
[2] A. Ciorba, L. Astolfi, C. Jolly, A. Marini, Review paper: Cochlear Implants and Inner Ear Based Therapy, Eur J Nanomed 2(2) (2009) 25-28.
[3] A. Ciorba, L. Astolfi, A. Martini, Otoprotection and inner ear regeneration, Audiol Med 6(3) (2008) 170-175.
[4] K. Oshima, S. Suchert, N.H. Blevins, S. Heller, Curing hearing loss: Patient expectations, health care practitioners, and basic science, J Commun Disord 43(4) (2010) 311-8.
[5] B.J. Copeland, H.C. Pillsbury, 3rd, Cochlear implantation for the treatment of deafness, Annual review of medicine 55 (2004) 157-67.
[6] K. Gfeller, C. Turner, M. Mehr, G. Woodworth, R. Fearn, J.F. Knutson, S. Witt, J. Stordahl, Recognition of familiar melodies by adult cochlear implant recipients and normal-hearing adults, Cochlear Implants Int 3(1) (2002) 29-53.
[7] B.J. Gantz, C. Turner, K.E. Gfeller, M.W. Lowder, Preservation of hearing in cochlear implant surgery: advantages of combined electrical and acoustical speech processing, Laryngoscope 115(5) (2005) 796-802.
[8] S. Danti, Boron nitride nanotubes as nanotransducers, in: G. Ciofani and V. Mattoli (Eds.), Boron Nitride Nanotubes in Nanomedicine, Elsevier Inc. 2016, pp. 123-38.
[9] J. Chang, M. Dommer, C. Chang, L. Lin, Piezoelectric nanofibers for energy scavenging applications, Nano Energy 1(3) (2012) 356-371.
[10] N. Mukherjee, R.D. Roseman, Considerations in the development of a piezoelectric transducer cochlear implant, Mater Res Soc Symp Proc 604 (2000) 79-84.
[11] N. Mukherjee, R.D. Roseman, J.P. Willging, The piezoelectric cochlear implant: concept, feasibility, challenges, and issues, J Biomed Mater Res 53(2) (2000) 181-7.
[12] N. Mukherjee, A. Shukla, A. Dwivedi, R.D. Roseman, D.F. Thompson, Vibrational and Acoustic Studies of Bending Mode Piezoelectricity in Millimeter Size Polyvinylidene Fluoride Cantilevers, in: Y. Bar-Cohen (Ed.) San Diego, CA, 2003, pp. 309-318.
[13] G. Von Bekesy, Travelling waves as frequency analysers in the cochlea, Nature 225(5239) (1970) 1207-1209.
[14] H. Shintaku, T. Nakagawa, D. Kitagawa, H. Tanujaya, S. Kawano, J. Ito, Development of piezoelectric acoustic sensor with frequency selectivity for artificial cochlea, Sens Actuators A Phys 158(2) (2010) 183-192.
[15] R.G. Kepler, R.A. Anderson, Piezoelectricity and pyroelectricity in polyvinylidene fluoride, J Appl Phys 49(8) (1978) 4490-4494.
[16] C.K. Purvis, P.L. Taylor, Piezoelectricity and pyroelectricity in polyvinylidene fluoride: Influence of the lattice structure, J Appl Phys 54(2) (1983) 1021-1028.
[17] T. Inaoka, H. Shintaku, T. Nakagawa, S. Kawano, H. Ogita, T. Sakamoto, S. Hamanishi, H. Wada, J. Ito, Piezoelectric materials mimic the function of the cochlear sensory epithelium, Proc Natl Acad Sci U S A 108(45) (2011) 18390-5.
[18] L.B. Kong, T.S. Zhang, J. Ma, F. Boey, Progress in synthesis of ferroelectric ceramic materials via high-energy mechanochemical technique, Prog Mater Sci 53(2) (2008) 207-322.
[19] G. Ciofani, S. Danti, L. Ricotti, D. D'Alessandro, S. Moscato, V. Mattoli, Applications of Piezoelectricity in Nanomedicine, in: G. Ciofani, A. Menciassi (Eds.), Piezoelectric Nanomaterials for Biomedical Applications, Springer Berlin Heidelberg 2012, pp. 213-238.
[20] G. Ciofani, L. Ricotti, V. Mattoli, Preparation, characterization and in vitro testing of poly(lactic-co-glycolic) acid/barium titanate nanoparticle composites for enhanced cellular proliferation, Biomedical microdevices 13(2) (2011) 255-66.

[21] G.G. Genchi, L. Ceseracciu, A. Marino, M. Labardi, S. Marras, F. Pignatelli, L. Bruschini, V. Mattoli, G. Ciofani, P(VDF-TrFE)/BaTiO3 Nanoparticle Composite Films Mediate Piezoelectric Stimulation and Promote Differentiation of SH-SY5Y Neuroblastoma Cells, Adv Healthc Mater 5(14) (2016) 1808-20.
[22] J.M. Corey, D.Y. Lin, K.B. Mycek, Q. Chen, S. Samuel, E.L. Feldman, D.C. Martin, Aligned electrospun nanofibers specify the direction of dorsal root ganglia neurite growth, J Biomed Mater Res A 83(3) (2007) 636-45.
[23] Q.P. Pham, U. Sharma, A.G. Mikos, Electrospinning of polymeric nanofibers for tissue engineering applications: a review, Tissue Eng 12(5) (2006) 1197-211.
[24] T.J. Sill, H.A. von Recum, Electrospinning: applications in drug delivery and tissue engineering, Biomaterials 29(13) (2008) 1989-2006.
[25] D. Li, Y. Xia, Electrospinning of Nanofibers: Reinventing the Wheel?, Adv Mater 16(14) (2004) 1151-1170.
[26] C. Mota, D. Puppi, D. Dinucci, C. Errico, P. Bartolo, F. Chiellini, Dual-Scale Polymeric Constructs as Scaffolds for Tissue Engineering, Materials 4(3) (2011) 527-542.
[27] C. Mota, S. Danti, D. D'Alessandro, L. Trombi, C. Ricci, D. Puppi, D. Dinucci, M. Milazzo, C. Stefanini, F. Chiellini, L. Moroni, S. Berrettini, Multiscale fabrication of biomimetic scaffolds for tympanic membrane tissue engineering, Biofabrication 7(2) (2015) 025005.
[28] G. Ciofani, S. Danti, D. D'Alessandro, S. Moscato, M. Petrini, A. Menciassi, Barium Titanate Nanoparticles: Highly Cytocompatible Dispersions in Glycol-chitosan and Doxorubicin Complexes for Cancer Therapy, Nanoscale research letters 5(7) (2010) 1093-101.
[29] C.V. Chanmal, J.P. Jog, Electrospun PVDF/BaTiO3 nanocomposites: polymorphism and thermal emissivity studies, Int J Plast Technol 15(S1) (2011) 1-9.
[30] S.F. Mendes, C.M. Costa, C. Caparros, V. Sencadas, S. Lanceros-Mendez, Effect of filler size and concentration on the structure and properties of poly(vinylidene fluoride)/BaTiO3 nanocomposites, J Mater Sci 47(3) (2012) 1378-1388.
[31] T. Bhimasankaram, S.V. Suryanarayana, G. Prasad, Piezoelectric polymer composite materials, Curr Sci India 74(11) (1998) 967-976.
[32] S. Danti, C. Mota, D. D'Alessandro, L. Trombi, C. Ricci, S.L. Redmond, A. De Vito, R. Pini, R.J. Dilley, L. Moroni, S. Berrettini, Tissue engineering of the tympanic membrane using electrospun PEOT/PBT copolymer scaffolds: A morphological in vitro study, Hearing Balance Commun 13(4) (2015) 133-147.
[33] L. Trombi, L. Mattii, S. Pacini, D. D'Alessandro, B. Battolla, E. Orciuolo, G. Buda, R. Fazzi, S. Galimberti, M. Petrini, Human autologous plasma-derived clot as a biological scaffold for mesenchymal stem cells in treatment of orthopedic healing, J Orthop Res 26(2) (2008) 176-83.
[34] J. Xie, M.R. MacEwan, X. Li, S.E. Sakiyama-Elbert, Y. Xia, Neurite outgrowth on nanofiber scaffolds with different orders, structures, and surface properties, ACS Nano 3(5) (2009) 1151-9.
[35] S.-S. Choi, Y.S. Lee, C.W. Joo, S.G. Lee, J.K. Park, K.-S. Han, Electrospun PVDF nanofiber web as polymer electrolyte or separator, Electrochim Acta 50(2–3) (2004) 339-343.
[36] A. Baji, Y.-W. Mai, X. Du, S.-C. Wong, Improved Tensile Strength and Ferroelectric Phase Content of Self-Assembled Polyvinylidene Fluoride Fiber Yarns, Macromol Mater Eng 297(3) (2012) 209-213.
[37] W.A. Yee, M. Kotaki, Y. Liu, X.H. Lu, Morphology, polymorphism behavior and molecular orientation of electrospun poly(vinylidene fluoride) fibers, Polymer 48(2) (2007) 512-521.
[38] T. Wang, T.U. Luu, A. Chen, M. Khine, W.F. Liu, Topographical modulation of macrophage phenotype by shrink-film multi-scale wrinkles, Biomater Sci 4(6) (2016) 948-52.
[39] P. Viswanathan, M.G. Ondeck, S. Chirasatitsin, K. Ngamkham, G.C. Reilly, A.J. Engler, G. Battaglia, 3D surface topology guides stem cell adhesion and differentiation, Biomaterials 52 (2015) 140-7.
[40] W.E. Teo, S. Ramakrishna, A review on electrospinning design and nanofibre assemblies, Nanotechnology 17(14) (2006) R89-R106.

[41] J.A. Matthews, G.E. Wnek, D.G. Simpson, G.L. Bowlin, Electrospinning of collagen nanofibers, Biomacromolecules 3(2) (2002) 232-8.
[42] N. Bhattarai, D. Edmondson, O. Veiseh, F.A. Matsen, M. Zhang, Electrospun chitosan-based nanofibers and their cellular compatibility, Biomaterials 26(31) (2005) 6176-6184.
[43] B. Sundaray, V. Subramanian, T.S. Natarajan, R.Z. Xiang, C.C. Chang, W.S. Fann, Electrospinning of continuous aligned polymer fibers, Appl Phys Lett 84(7) (2004) 1222-1224.
[44] A. Theron, E. Zussman, A.L. Yarin, Electrostatic field-assisted alignment of electrospun nanofibres, Nanotechnology 12(3) (2001) 384-390.
[45] R. Inai, M. Kotaki, S. Ramakrishna, Structure and properties of electrospun PLLA single nanofibres, Nanotechnology 16(2) (2005) 208-13.
[46] P. Katta, M. Alessandro, R.D. Ramsier, G.G. Chase, Continuous electrospinning of aligned polymer nanofibers onto a wire drum collector, Nano Lett 4(11) (2004) 2215-2218.
[47] C. Ayres, G.L. Bowlin, S.C. Henderson, L. Taylor, J. Shultz, J. Alexander, T.A. Telemeco, D.G. Simpson, Modulation of anisotropy in electrospun tissue-engineering scaffolds: Analysis of fiber alignment by the fast Fourier transform, Biomaterials 27(32) (2006) 5524-34.
[48] F. Croisier, A.S. Duwez, C. Jerome, A.F. Leonard, K.O. van der Werf, P.J. Dijkstra, M.L. Bennink, Mechanical testing of electrospun PCL fibers, Acta biomaterialia 8(1) (2012) 218-24.
[49] B.F. Zagadou, P.E. Barbone, D.C. Mountain, Elastic properties of organ of Corti tissues from point-stiffness measurement and inverse analysis, J Biomech 47(6) (2014) 1270-7.
[50] L. Astolfi, E. Simoni, A. Martini, OC-k3 cells, an in vitro model for cochlear implant biocompatibility, Hearing Balance Commun 13(4) (2015) 166-174.